JOURNAL OF GEOPHYSICAL RESEARCH, VOL. 103, NO. A11, PAGES 26,805–26,812, NOVEMBER 1, 1998

Magnesium isotopic composition as observed with the CELIAS/MTOF experiment on the SOHO spacecraft

H. Kucharek,[1] F. M. Ipavich,[2] R. Kallenbach,[3] P. Bochsler,[4] D. Hovestadt,[1] H. Grünwaldt,[5] M. Hilchenbach,[5] W. I. Axford,[5] H. Balsiger,[4] A. Bürgi,[6] M. A. Coplan,[2] A. B. Galvin,[2] J. Geiss,[3] F. Gliem,[7] G. Gloeckler,[2] K. C. Hsieh,[8] D. J. Judge,[9] B. Klecker,[1] M. A. Lee,[10] S. Livi,[5] G. G. Managadze,[11] E. Marsch,[5] E. Möbius,[10] M. Neugebauer,[12] H. S. Ogawa,[9] K.-U. Reiche,[7] M. Scholer,[1] M. I. Verigin,[11] B. Wilken,[5] and P. Wurz[4]

Abstract. Solar wind abundance ratios of magnesium isotopes measured with the high resolution Mass Time-of-Flight spectrometer (MTOF) of the Charge, Element, and Isotope Analysis System (CELIAS) experiment on board the Solar and Heliospheric Observatory (SOHO) are presented. MTOF, as part of CELIAS, is, because of its high time and mass resolution, an excellent tool for isotope abundance measurements in the solar wind. From the data analysis we have found that the isotopic composition of magnesium in the solar wind agrees with the terrestrial composition within the experimental uncertainty. We have obtained isotopic ratios of $^{24}Mg/^{25}Mg = 7.7 \pm 0.4$ and $^{24}Mg/^{26}Mg = 7.0 \pm 0.5$. These values are consistent with the terrestrial values of $^{24}Mg/^{25}Mg = 7.90 \pm 0.01$ and $^{24}Mg/^{26}Mg = 7.17 \pm 0.03$. Furthermore, these investigations also show that with the given uncertainties the abundance ratios do not vary significantly within a solar wind velocity range from 375 km/s to 530 km/s.

1. Introduction

The knowledge of the isotopic composition of solar system material is essential for the study of the origin of the elements in stars and the formation of the solar system. Analysis of solar particle isotopic abundances provides the only tool to obtain information on the isotopic composition of the outer convective zone of the Sun [*Meyer*, 1992] and, finally, about the nuclidic abundances of the primordial solar nebula [*Clayton*, 1993]. Among the wide variety of elements in solar system bodies, there are the so-called refractory (nonvolatile) elements. These elements will not undergo isotopic fractionation by loss processes from an early solar nebula. Magnesium is one of these elements, and it has three stable isotopes, all with fractional abundances of more than 10%. The isotopic abundance ratios of this element cannot be modified by conventional hydrogen burning during the lifetime of the Sun. For all these reasons, it can be regarded as an isotopic "standard" to study isotope fractionation effects on solar wind particles on their way from the source region in the photosphere of the Sun to the interplanetary medium.

The solar system isotopic composition distributions were first studied using terrestrial, lunar, and meteoritic material. Only for the noble gases He, Ne, and Ar could the isotopic composition of the solar wind be measured in situ by the Apollo foil experiments [*Geiss et al.*, 1972]. Later, satellite-borne spectrometers which measure solar energetic particles (SEPs) provided a tool for direct sampling of solar material. Results of the IMP 8 [*Dietrich and Simpson*, 1979] and ISEE 3 missions have shown that in SEP events the $^{22}Ne/^{20}Ne$ ra-

[1]Max-Planck-Institut für extraterrestrische Physik, Garching, Germany.
[2]Department of Physics and Astronomy, University of Maryland, College Park.
[3]International Space Science Institute, Bern.
[4]Physikalisches Institut, Universität Bern, Bern.
[5]Max-Planck-Institut für Aeronomie, Katlenburg-Lindau, Germany.
[6]Arias Luftreinhaltung und Umweltberatung, Bern.
[7]Institut für Datenverarbeitung, Technische Universität Braunschweig, Germany.
[8]Department of Physics, University of Arizona, Tucson.
[9]Space Science Center, University of Southern California, Los Angeles.
[10]Institute for the Study of Earth, Ocean and Space, University of New Hampshire, Durham.
[11]Institute for Space Physics, Moscow, Russia.
[12]Jet Propulsion Laboratory, Pasadena, California.

Paper number 98JA02542.
0148-0227/98/98JA-02542$09.00

tio was considerably larger than that in the solar wind [*Mewaldt et al.*, 1979]. On the other hand, more recent measurements by *Selesnick et al.* [1993] with the Solar Anomalous Mangetospheric Particle Explorer (SAMPEX) show that the observed $^{22}Ne/^{20}Ne$ ratio during two large solar particle events in October and November 1992 is consistent with the solar wind value. The authors conclude that the neon isotope composition varies from event to event. SEP measurements of the $^{25}Mg/^{24}Mg$ and $^{26}Mg/^{24}Mg$ ratios were found to be consistent with terrestrial and meteoritic abundances [*Mewaldt et al.*, 1981a,b, *Dietrich and Simpson*, 1981; *Selesnick et al.*, 1993].

In the present paper we concentrate on isotope measurements in the solar wind. The majority of solar particles is carried in the solar wind, whereas solar energetic particles (a minor fraction) undergo a complicated sequence of processes. Various fractionation effects at different sites between the solar surface and the interplanetary plasma cause variations in elemental and isotopic composition. Solar wind particles, for example, are ionized in the chromosphere and the transition region. Neutrals diffuse from the photosphere into the chromosphere, where they get ionized depending on their element specific first ionization time [*Geiss and Bochsler*, 1985] and will then be separated from the ions, which are uplifted because of Coulomb-drag by the proton gas. From the steady state model of *Marsch et al.* [1995] a very small enrichment of magnesium isotopes (^{24}Mg relative to ^{26}Mg) of the order of <1.001 is expected from this process.

Element or isotope fractionation can also be caused by inefficient Coulomb coupling in the inner corona. This is the strongest effect on the fractionation of Mg isotopes and occurs in streamer type solar wind with strong superradial expansion in the inner corona [*Bürgi*, 1991a,b; *Bodmer and Bochsler*, 1996]. This model predicts a maximum isotopic fractionation factor of 1.03 for the case of $^{24}Mg/^{26}Mg$. The given factor indicates that the heavier isotopes are depleted with respect to ^{24}Mg. The model of *Bodmer and Bochsler* [1996] takes into account effects which occur between the upper corona and the interplanetary space near 1 AU and reproduces observed He/H variations consistent with observations. Therefore a precise measurement of element and isotopic abundances, and in this case magnesium isotopic abundances, provides a unique opportunity to derive constraints on fractionation effects of solar wind particles on their way from the source region in the photosphere to the interplanetary medium.

Much stronger fractionation mechanisms are known for the SEPs (e.g., for ^{3}He-rich events). In the solar atmosphere, element and isotope fractionation may occur by resonant wave particle interaction [*Mason et al.*, 1994]. In the interplanetary medium, fractionation may occur where shock acceleration processes can enrich or deplete particle abundances according to their mass to charge ratio [*Mewaldt and Stone*, 1989]. Fractionation resulting from the latter process, however, may cancel out in long-term averages of isotopic abundances in the SEPs. The comparison of solar wind isotope abundances with solar particle isotopic abundances therefore provides a very good tool to obtain information on acceleration processes and the isotopic composition of the outer convective zone of the Sun.

2. Observation With SOHO/CELIAS/MTOF

The Solar Heliospheric Observatory (SOHO) has been realized by the European Space Agency (ESA) and NASA in the framework of the International Solar Terrestrial Program (ISTP). The Mass Time-of-Flight (MTOF) sensor of the Charge, Element, and Isotope Analysis System (CELIAS) on board SOHO is an isochronous time-of-flight mass spectrometer with a high mass resolution $M/\Delta M$, which allows the resolution of almost all isotopes of the solar wind elements up to 60 atomic mass units.

The CELIAS experiment package was jointly developed by five hardware institutions under the lead of the Max-Planck-Institut für extraterrestrische Physik in Garching, Germany. The MTOF sensor was developed under the lead of the Space Physics Group of the University of Maryland. The entrance system of the sensor was built at INTEC in Bern under the guidance of the physics group of the University of Bern, whereas the Data Processing Unit (DPU) was built at the Technical University of Braunschweig.

Since the sensor is described in detail elsewhere [*Hovestadt et al.*, 1995; *Kallenbach et al.*, 1997], we will only briefly review its basic function. Futhermore, many details concerning the following data analysis are described in the paper of *Kallenbach et al.*, [1997]. Highly charged solar wind ions enter the Wide Angle Variable Energy (WAVE) entrance system, which is designed to suppress the solar wind proton flux and the solar UV flux. After the remaining ions leave the WAVE they can be accelerated or decelerated before they enter the V-shaped VMASS isochronous time-of-flight spectrometer. At the entrance to VMASS the ions pass through a thin carbon foil where secondary electrons are released, which produces a start signal at the Electron Microchannel Plate (EMCP). After passing through the carbon foil, particles are mostly neutral or singly ionized [*Bürgi*, 1990; *Gonin et al.*, 1992]. In VMASS a hyperbola deflection electrode and a V-shaped ground electrode generate an electrostatic harmonic potential so that the time of flight (TOF) in the detector is proportional to $(M/Q)^{1/2}$, where M is the mass and Q is the charge of an ion after passing through the thin carbon foil. Finally, the TOF is measured between the start and the stop signal which the ion generates at the Ion Microchannel Plate (IMCP) detector. In Appendices A and B we will discuss the essential instrument function defining the detection efficiency of the MTOF sensor for the magnesium isotopes.

3. Evaluation of the Time-Of-Flight Spectra

For the analysis of the TOF spectra, pulse height analysis (PHA) words as well as MT1 spectra from onboard analysis have been used. One PHA word contains the start amplitude, two stop amplitudes, the time of flight, and an identifier. Every ion event carries an identifier which indicates whether the event is an ion or neutral event. This "flag" identifies the range into which the ion event has been classified by the DPU. The MT1 data are classified on board into 1024 TOF channels and are available on a 5-min basis (see *Kallenbach et al.* [1997] for a detailed description of these data). The instrument settings such as the voltage V_f (float potential for post acceleration/deceleration of the solar wind ions) and V_w (the deflection voltage of the entrance system WAVE) have been taken from the housekeeping data. The data from the Proton Monitor (for details see *Ipavich et al.* [1998]) have been used to extract the bulk velocity of the solar wind $v_{\rm bulk}$ and its thermal speed $v_{\rm therm}$. These data are available with a time resolution of 5-min. The time series of PHA words as well as the MT1 spectra for the magnesium isotopes have then been selected and ordered into classes of these parameters. For the investigations described below we have used only data from measurements at negative V_f (i.e. postaccelerated positive particles). These groups of TOF spectra have been selected according to their detection efficiency ratio $\eta(^{25}\mathrm{Mg}, U_W, V_f, v_{\rm bulk}, v_{\rm therm})$ divided by $\eta(^{24}\mathrm{Mg}, U_W, V_f, v_{\rm bulk}, v_{\rm therm})$ for $^{25}\mathrm{Mg}/^{24}\mathrm{Mg}$ and $^{26}\mathrm{Mg}/^{24}\mathrm{Mg}$, respectively. The data have also been filtered according to the particle identifier. For the analysis we have used only those events which have shown the lowest background originating from scattered neutrals. Figure 1 shows a spectrum of PHA words which is a histogram of data from the first 200 days (20-220) in 1996, selected using the criterion that the detection efficiency ratio must lie between 0.85 and 1.15. The selected data are shown in Figure 1 by the diamond symbols, whereas the solid line represents a fitted function which is described below.

3.1. Analysis of the PHA and MT1 Data

For the analysis of the TOF spectra we have used the PHA as well as the MT1 data, which we have analyzed as described below. For the spectrum (Figure 1 shows a spectrum obtained from PHA words), four time-of-flight channels have been binned, and the data have then been smoothed with a Gaussian filter which corresponds to the half width of the TOF resolution. The reduction of the mass resolution is only about 12%. All three isotopes of magnesium are clearly visible, as are the neighboring elements at the low and the high end of the TOF spectrum. It exhibits that different isotopes show different peak shapes. One of the main reasons for this effect is that different isotopes have different trajectories inside the detector, which in turn may lead to a different shape of the TOF distribution [see also

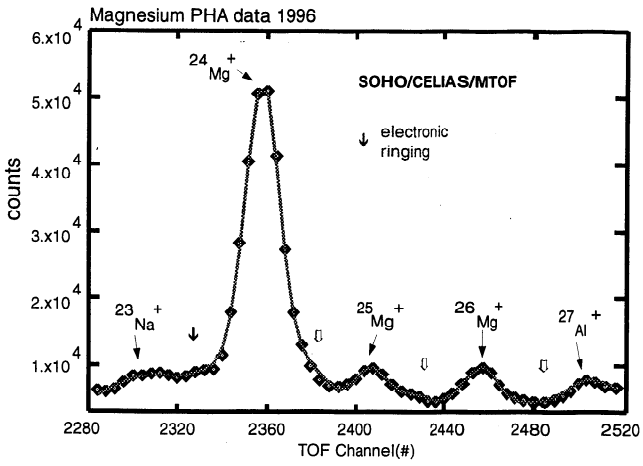

Figure 1. Time-of-flight spectrum for the first 200 days (days 20-220) of 1996 derived from pulse height analysis (PHA) words and filtered with respect to an expected instrument bias factor in a window of $0.85 < f_{26/24} < 1.15$. For Figure 1, four time-of-flight (TOF) channels have been binned together, and the data have been smoothed. The data points are represented by diamonds, whereas the full line shows the fit function.

Kallenbach et al., 1998]. For the analysis of the TOF spectra we have used the best fit to the data. During the analysis it turned out that a Lorentzian type function shows the best results for the magnesium isotopes, which is different from the fit function used for the analysis of neon isotopes [*Kallenbach et al.*, 1997]. However, since only ratios of isotope abundances are determined the uncertainties are rather small.

All three peaks of $^{24}\mathrm{Mg}$, $^{25}\mathrm{Mg}$, and $^{26}\mathrm{Mg}$ are described by the same Lorentzian function with an identical width. The position and the heights of the peaks have been fitted. The magnesium spectrum model function is a sum of functions which can be divided into the following parts:

$$F(x) = \sum_i \frac{A_i}{(1+\frac{1}{2}(\frac{x-x0_i}{b_i})^2 * \lambda_i)^{\lambda_i}} + \sum_n \frac{A_n}{(1+\frac{1}{2}(\frac{x-x0_n}{b_n})^2 * \lambda_n)^{\lambda_n}} + \sum_r \frac{A_r}{(1+\frac{1}{2}(\frac{x-x0_r}{b_r})^2 * \lambda_r)^{\lambda_r}} + Cx + D \quad (1)$$

The spectrum is modeled as a sum of Lorentzian functions, where the indices represent the different peaks and x represents the time of flight channels. The first term of equation (1) describes the peaks of the magnesium isotopes. Here the amplitudes are denoted by A_i, whereas the peak positions in the spectrum are given by $x0_i$ for the isotopes $^{24}\mathrm{Mg}$,$^{25}\mathrm{Mg}$, and $^{26}\mathrm{Mg}$. The half widths b_i of the functions have been fitted to the spec-

tra but are the same for all the isotopes. The parameter λ_i, which describes the deviation from a lorentzian function, has also been fitted to the time-of-flight spectrum and has been assumed to be independent of mass. In addition, we have fitted the neighboring elements Na and Al (second term of (1)) as well as the peaks which originate from an electronic ringing effect (third term of (1)). This is a systematic instrumental effect. The origin of this effect arises from reflected start signals at start MCP. These peaks are observable at about 25 to 35 channels to the left of any well-resolved time-of-flight peak in the MTOF mass spectrum. The amliptude of these peaks depends on the number of electrons emitted from the carbon foil. The background is described by a linear function in the time-of-flight (channel number) x and by two constants C and D (last term of (1)). The magnesium peaks are resolved with very good statistics; therefore the error bars for the statistical uncertainty are not shown in Figure 1.

3.2. Analysis of the Time-Of-Flight Spectra

So far, we have not considered statistical and instrumental effects in our investigations of the time-of-flight spectra. Figure 2 shows the total counts for the different magnesium isotopes and the abundance ratios for $^{24}Mg/^{25}Mg$ and $^{24}Mg/^{26}Mg$ as a function of the instrument bias. These ratios have been corrected for the instrument bias derived from the parameterized instrument function. The best counting statistic is obtained at instrument bias factors between 1 and 1.05. This is reasonable because more particles are collected on the maximum of the instrument response function. Figures 1b and 1c show the corrected counting rate ratios for $^{24}Mg/^{25}Mg$ as well as for $^{24}Mg/^{26}Mg$ as a function of the instrument bias factor; the solid line shows a linear regression fit to the data points. The ratios show almost no variation with the instrument bias. Over a range, $0.95 < f_{24/26} < 1.05$, the fit function is flat, and we obtain an uncertainty of about 2% per unit instrument bias factor. This demonstrates that the abundance ratios which are corrected for the instrument bias derived from the parameterized instrument function are independent from the instrument bias factor. Deviations may occur within the absolute calibration error [see *Kallenbach et al.*, 1997]. From the statistical analysis we obtain for the total range of the instrument bais factor a corrected mean value of 7.7 ± 0.4 for $^{24}Mg/^{25}Mg$ and 7.0 ± 0.5 for $^{24}Mg/^{26}Mg$.

The isotope abundance ratios have been studied for different solar wind parameters. Figure 3 shows the different ratios for the magnesium isotopes at different solar wind velocities. The data (represented by dia-

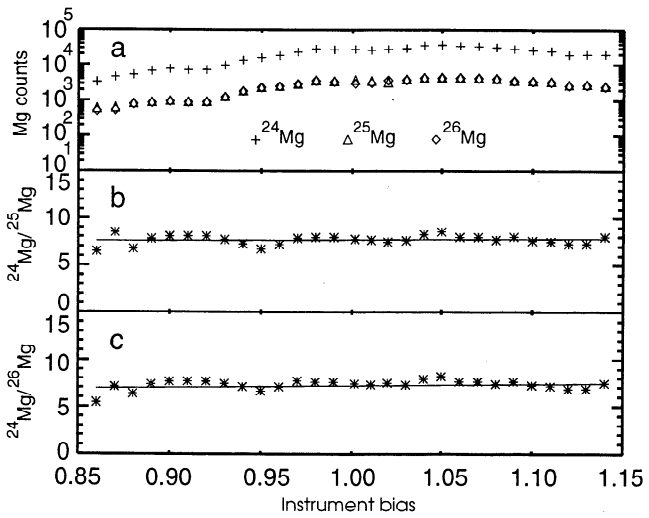

Figure 2. The total counts for (a) $^{24,25,26}Mg$ as well as (b) the $^{24}Mg/^{26}Mg$ and (c) the $^{24}Mg/^{25}Mg$ isotope ratio corrected by the instrument bias factor as a function of the calculated instrument bias factor. The solid line shows a fit to the data.

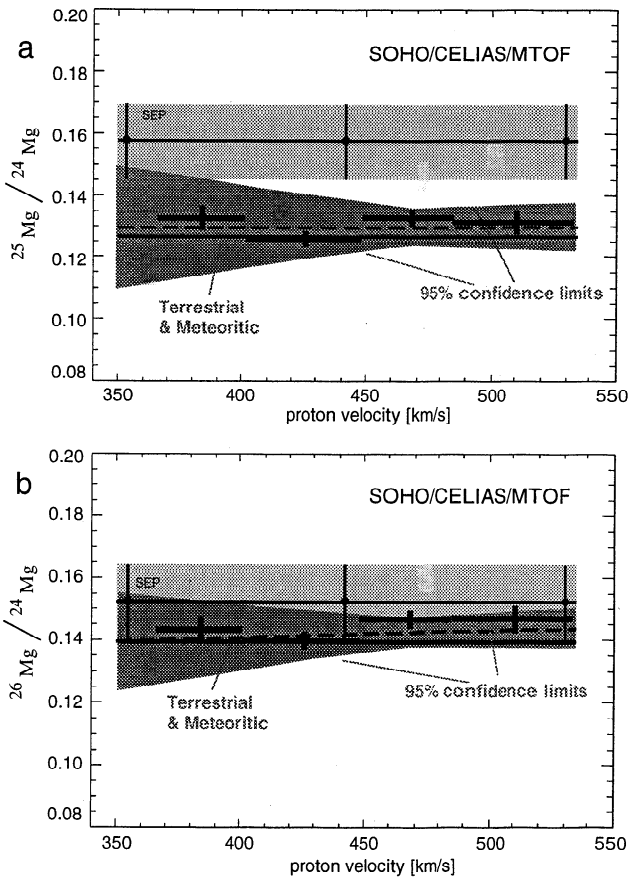

Figure 3. Solar wind abundance of the magnesium isotope ratios (a) $^{25}Mg/^{24}Mg$ and (b) $^{26}Mg/^{24}Mg$ as a function of the solar wind speed. Also shown is the corresponding ratio for solar energetic particles (SEPs) and for the terrestrial and meteoritic abundance. The light gray shaded areas indicate the error range for isotiope ratios for SEPs. The dark gray shaded areas indicate the 95% confidence limits for the measured magnesium isotope ratios. The error bars shown for the measured data points represent the statistical errors only. The calibration error (not shown here) is conservatively estimated at about 6%.

monds) are close to the terrestrial and meteoritic values [*Anders and Grevesse*, 1989]. Also shown in Figures 3a and 3b are the ratios obtained from measurements of solar energetic particles events from October and November 1992 [*Selesnick et al.*, 1993] where average values of $^{25}Mg/^{24}Mg = 0.157 \pm 0.012$ and $^{26}Mg/^{24}Mg = 0.152 \pm 0.012$ have been found. In both Figures 3a and 3b the ratios derived from the MTOF measurements are close to the terrestrial ratios. Furthermore, the terrestrial ratios are within the 95% confidence limits (dark gray shaded area). The dashed line shows the regression with the data points. For this investigation, 320 days of data from 1996 have been used, starting from day 20 and ending with day 340 in 1996. The regression lines indicate a slight increase for higher solar wind velocities (more visible for $^{26}Mg/^{24}Mg$); however, this increase is not statistically significant.

4. Results and Discussion

Compared to other missions, for example WIND, much improved counting statistics have been achieved. This is due to the three-axis stabilized SOHO spacecraft that provides the possibility to continuously detect the solar wind and is also due to the wideband energy-per-charge filter WAVE.

The magnesium isotope abundances of the solar wind derived in this paper agree well with the terrestrial values [*Anders and Grevesse*, 1989] and with other in situ measurements such as WIND/MASS [*Bochsler et al.*, 1995, 1997]. These first results obtained with CELIAS/MTOF show no significant dependence of the magnesium isotope abundance on the solar wind within a solar wind range from 375 km/s to 530 km/s.

This, however, does not exclude quantitative fractionation which may be caused by the efficiency of Coulomb friction in different solar wind sources. More data and the analysis of more isotopes (such as Si, etc.) may help to study those physical processes.

Appendix A: The Geometry Factor

The geometry factor is defined by the ion optical transmission of the entrance system. This factor is the most crucial instrument property when deriving elemental or isotopic abundances. In order to determine the detection efficiency, the solar wind velocity distribution has to be convoluted with the instrument acceptance in entrance angles α and β and the energy per charge of the solar wind ions E/Q. The angle α is in the ecliptic, and β is perpendicular to it. Figure 4 shows the acceptance function of the entrance system including the transmission onto the carbon foil of the time-of-flight sensor for two different float potentials V_f for Mg^{+10} in the E/Q - α plane. The gray-shaded contours show 20%, 40%, 60%, and 80% level in comparison with the maximum effective area of 3.2 mm^2 at $V_f = 0$ kV. Overlaid is a typical normalized solar wind distribution at the levels 0.05, 0.35, 0.65, and 0.95. As shown by *von Steiger et al.* [1995], all He and heavy ions have the same velocity. Therefore we assume that all magnesium isotopes travel at about the same solar wind bulk velocity so that the heaviest isotope ^{26}Mg has the highest energy per charge E/Q for both float potentials. For solar wind distributions with maxima close to a steep slope of the instrument response function, the integrated efficiencies can differ by about a factor of 2. Therefore it is important to filter the flight data with respect to the instrument discrimination.

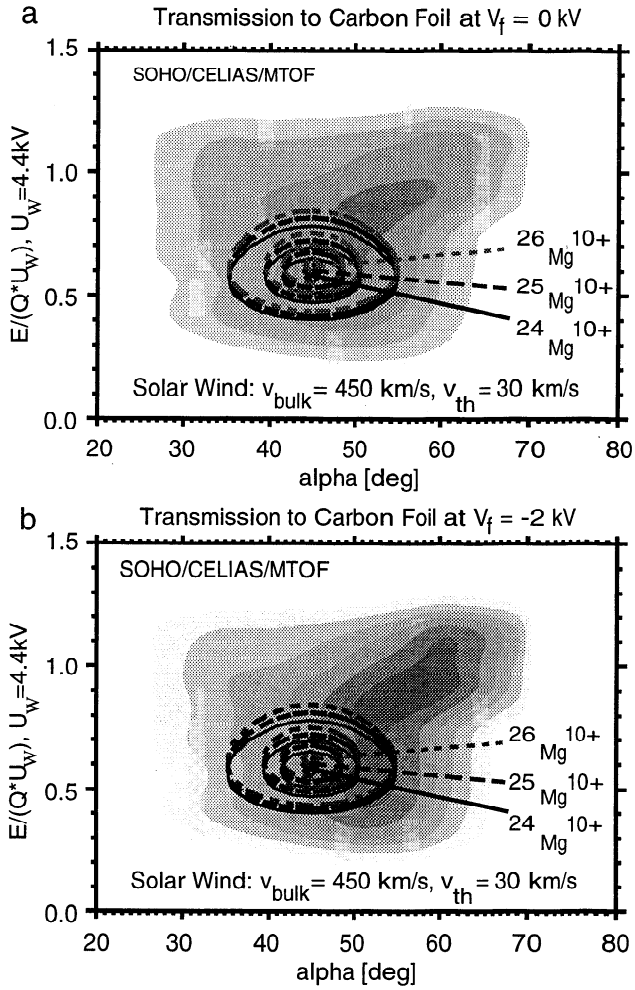

Figure 4. (a) Acceptance function of the entrance system including carbon foil transmission as a function of energy-per-charge E/Q of solar wind ions and the entrance angle in the ecliptic α for $V_f = 0$ kV. Superimposed is a typical normalized solar wind distribution of $^{24}Mg^{+10}$ (solid line), $^{25}Mg^{+10}$ (dashed line), and $^{26}Mg^{+10}$ (dash-dotted line) at the levels 0.05, 0.35, 0.65, and 0.95. The gray-shaded contours show the 20%, 40%, 60%, and 80% level in comparison with the maximum effective area of 3.2 mm^2. (b) Acceptance function of the entrance system for $V_f = -2$ kV. The contour level spacing is the same as in Figure 4a, but because of the negative postacceleration voltage which focuses the ions onto the C foil, the effective area can be larger than 3.2 mm^2. Shown are six contour levels, where the highest level is 120%.

Appendix B: The Detection Efficiencies

Since a magnesium ion beam was not available for the sensor calibration, we used a parameterized instrument function by interpolating the calibration data and model calculations of the neighboring elements Si and Ne. These parameterized instrument functions enable us to determine the detection efficiency and the instrument fractionation. Following the trajectory of a charged particle in the sensor from the entrance system to the stop MCP, we discuss the important effects which have an impact on fractionation and detection efficiency of magnesium isotopes.

B1. Start Efficiency

The start efficiency is determined by the secondary electron emission from the carbon foil, which depends on the element species and the ion velocity and the efficiency of the start MCP. These data are well reproduced by simulation calculations [*Ziegler et al.*, 1985] for the electronic stopping in a thin carbon foil with thickness of about 2.1 $\mu g/cm^2$. With these numbers we have found a relatively small isotopic discrimination of ^{26}Mg to ^{24}Mg for the front secondary electron detection assembly (SEDA) rate (FSR) as shown in Figure 5.

B2. Double Coincidence Efficiency

This efficiency is determined by effects at the carbon foil, by the ion optical transmission, and by the efficiency of the IMCP. The probability that an ion is detected is given by the ratio DCR/FSR (double coincidence rate/front SEDA rate). All statistical distribution functions for the energy loss and straggling, the angular scattering and the charge exchange probability of an isotope at the backside of the thin carbon foil, as well as the ion optical transmission inside VMASS have been taken into account. For more of those experimental details see *Kallenbach et al.* [1995, 1997]. In

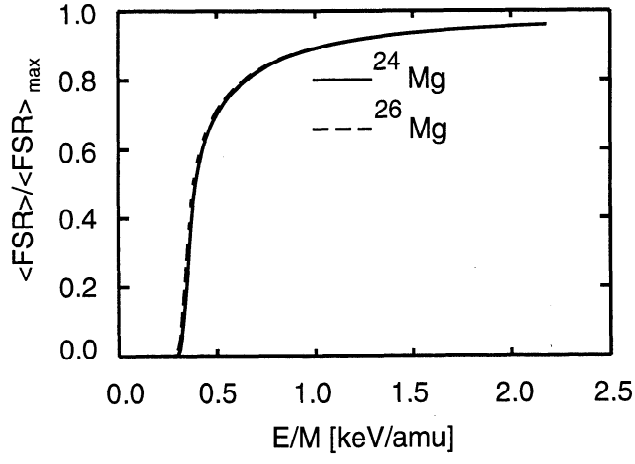

Figure 5. Model calculations for the front secondary electron detection assembly (SEDA) rate (FSR) as a function of energy per mass E/M. The solid line represents ^{24}Mg, whereas the dashed line represents ^{26}Mg.

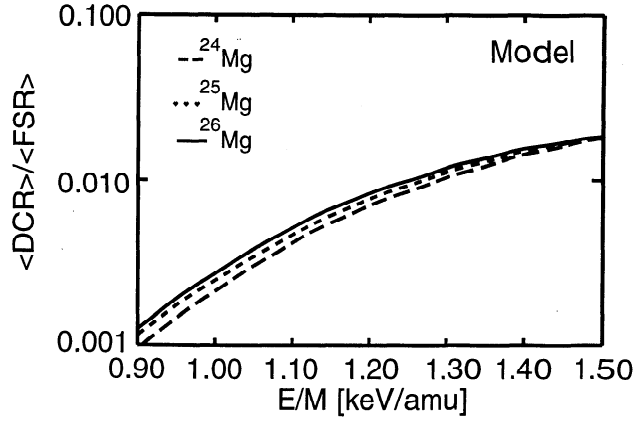

Figure 6. Double coincidence rate (DCR) over FSR as a function of E/M for ^{24}Mg, ^{25}Mg, and ^{26}Mg at a hyperbola electrode voltage of 20.7 kV.

Figure 6 we show DCR/FSR for ^{24}Mg and ^{26}Mg as a function of energy per mass E/M. These graphs are the result of model calculations for a hyperbola voltage of 20.7 kV. The double coincidence efficiencies for the three isotopes vary from 0.0005 at low E/M to 0.02 at higher E/M. Instrument fractionation is slightly higher

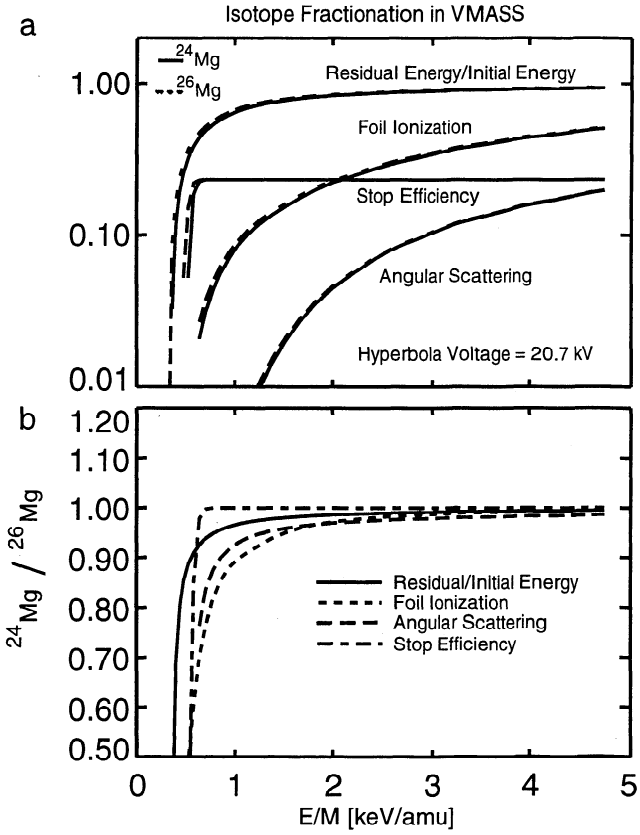

Figure 7. (a) Detailed summary plot of different effects in the carbon foil and in VMASS as a function of energy per mass for ^{24}Mg and ^{26}Mg. Shown is the relative energy loss in the C foil, the charge exchange efficiency, the stop efficiency, and the transmission due to angular scattering. Figure 7b shows the ratios of the corresponding ^{24}Mg and ^{26}Mg curves.

at lower E/M. A detailed summary of all these different physical effects in and at the carbon foil and in VMASS is shown in Figure 7. In Figure 7 the solid line represents ^{24}Mg and the dashed line represents ^{26}Mg (Figure 1a). Figure 1b shows the ratios of the corresponding ^{24}Mg and ^{26}Mg curves. At the same E/M, ^{26}Mg suffers less energy loss than ^{24}Mg, and therefore it has a slightly higher probability to release secondary electrons. This in turn leads to a higher probability of being detected on the VMASS stop MCP. Also, the angular scattering in the carbon foil is smaller for ^{26}Mg than for ^{24}Mg. Therefore the detection efficiency is slightly higher for ^{26}Mg compared to ^{24}Mg at the same value of E/M.

Acknowledgments. This work was supported by the Swiss National Science Foundation, by the PRODEX program of ESA, by NASA, and by DLR, Germany, contracts 500C9605 and 500C8905.

The Editor thanks Rudolf von Steiger and Mark E. Wiedenbeck for their assistance in evaluating this paper.

References

Anders, E., and N. Grevesse, Abundance of the elements: Meteoritic and solar, *Geochim. Cosmochim. Acta, 53*, 197-214, 1989.

Bochsler, P., M. Gonin, R. B. Sheldon, T. Zurbuchen, G. Gloeckler, A. B. Galvin, and D. Hovestadt, Elemental composition in the slow solar wind measured with the MASS instrument on WIND in *Solar Wind Eight: AIP Conference Proceedings*, pp. 199-202, AIP Press, Woodbury, N.Y. 1995.

Bochsler, P., H. Balsiger, R. Bodmer, O. Kern, T. Zurbuchen, G. Gloeckler, D. C. Hamilton, M. R. Collier, and D. Hovestadt, Limits to the efficiency of isotope fractionation processes in the solar wind derived from the magnesium isotope composition as observed with the WIND/MASS experiment, *Phys. Chem. Earth, 22*, 401-404, 1997.

Bodmer, R., and P. Bochsler, Fractionation of minor ions in the solar wind acceleration process (abstract), paper presented at meeting, Eur. Geophys. Soc., The Hague, Netherland, 1996.

Bürgi, A., Dynamics of alpha particles in coronal streamer type geometries, In *Solar Wind Seven: Proceedings of the 3rd COSPAR Colloquium, Goslar, Germany*, 333-336, Pergamon, Tarrytown, N.Y. 1991a.

Bürgi, A., Ion composition measurements, *Adv. Space. Res., 11*, 391-400, 1991b.

Bürgi, A., M. Oetliker, P. Bochsler, J. Geiss, and M. A. Coplan, Charge exchange of low-energy ions in thin carbon foils, *J. Appl. Phys., 68*, 2547-2554, 1990.

Clayton, R. N., Oxygen isotopes in meteorites, *Annu. Rev. Earth Planet. Sci., 21*, 115-149, 1993.

Dietrich, M. F., and J. A. Simpson, The isotopic and elemental abundances of neon nuclei accelerated in solar flares, *Astrophys. J., 231*, L91-L95, 1979.

Dietrich, M. F., and J. A. Simpson, The isotopic composition of magnesium nuclei in solar flares, *Astrophys. J., 245*, L41-L44, 1981.

Geiss, J., and P. Bochsler, Ion composition in the solar wind in relation to solar abundances, in *Isotopic Ratios in the Solar System* pp. 213-228 Cépaduès Éditions, Toulouse, France 1985.

Geiss, J., F. Bühler, H. Cerutti, P. Eberhardt and C. Filleux, Solar wind composition experiment, in *Apollo 16 Preliminaty Scientific Report, NASA Specical Publ. SP-315*, 14. 1, 1972.

Gonin, M., A. Bürgi, M. Oetliker, and P. Bochsler, Interaction of solar wind ions with thin carbon foils: Calibration of time-of-flight spectrometers, in *Proceedings of the First SOHO Workshop* Eur. Space Agency Spec. Publ., ESA SP-348, 381-384, 1992.

Hovestadt, D., et al., CELIAS - Charge, Element and Isotope Analysis System for SOHO, *Sol. Phys.*, 441-481, 1995.

Ipavich, F. M., et al., Solar wind measurements with SOHO: The CELIAS/MTOF proton monitor, J. Geophys. Res., 103(A8), 17,205-17,213, 1998.

Kallenbach, R., R. M. Gonin, and P. Bochsler, Charge exchange of B, C, O, Al, Si, S, Fe and Cl passing through thin carbon foils at low energies: Formation of negative ions, *Nucl. Instrum. Methods, Phys. Res. Sect. B 103*, 111-116., 1995.

Kallenbach, R., et al., Isotopic composition of solar wind neon measured by CELIAS/MTOF on board SOHO, *J. Geophys. Res. 102*, A12, 26,895-26,904, 1997.

Kallenbach, R., et al., Isotopic composition of solar wind calcium: First in situ measurement by CELIAS/MTOF on board SOHO, *Astrophys. J., 498*, L75-L78, 1998.

Marsch, E., R. von Steiger, and P. Bochsler, Element fractionation by diffusion in the solar chromosphere, *Astron. Astrophys., 301*, 261-276, 1995.

Mason, G. M., J. E. Mazur, and D. C. Hamilton, Heavy-ion isotopic anomalies in He-3 rich solar particle events, *Astrophys. J., 425*, 843-848, 1994.

Mewaldt, R. A., and E. C. Stone, Isotope abundances of solar coronal material derived from solar energetic particle measurements, *Astrophys. J., 337*, 959-963, 1989.

Mewaldt, R. A., J. D. Spalding, E. C. Stone, and R. E. Vogt, The isotopic composition of solar flare accelerated neon, *Astrophys. J., 231*, L97-L100, 1979.

Mewaldt, R. A., J. D. Spalding, E. C. Stone, and R. E. Vogt, The isotopic composition of solar flare accelerated magnesium, *Astrophys. J., 243*, L163-L165, 1981a.

Mewaldt, R. A., J. D. Spalding, E. C. Stone, and R. E. Vogt, The isotopic composition of low energy cosmic rays; *Proc. Int. Conf. Cosmic Rays, 17th, (Paris), 3*, 131-134, 1981b.

Meyer, J.-P., Element fractionation at work in the solar atmosphere, in *Origin and evolution of the elements*, Cambridge Univ. Press, New York 1992.

Selesnick, R. S., A. C. Cummings, J. R. Cummings, R. A. Lesks, R. A. Mewaldt, E. C. Stone, and T. T. von Rosenvinge, Coronal abundances of neon and magnesium isotopes from solar energetic particles, *Astrophys. J., 418*, L45-L48, 1993.

von Steiger, R., J. Geiss, G. Gloeckler, and A. B. Galvin, Kinetic properties of heavy ions in the solar wind from SWICS/ULYSSES, *Space Sci. Rev., 72*, 71-76, 1995.

Ziegler J. F., J. P. Biersack, and U. Littmark in *The stopping and range of ions in matter*, Pergamon, Tarrytown , N. Y., 1985.

W. I. Axford, H. Grünwaldt, M. Hilchenbach, E. Marsch, and B. Wilken, Max-Planck-Institut für Aeronomie, D-37189, Kaltenburg-Lindau, Germany.
(e-mail: gruenwaldt@linax1.dnet.gwdg.de

H. Balsiger, P. Bochsler, and P. Wurz, Physikalisches Institut, Universität Bern, CH-3012 Bern, Switzerland.
(e-mail: peter.wurz@soho.unibe.ch)

A. Bürgi, Arias Luftreinhaltung und Umweltberatung, CH-3012 Bern, Switzerland.
(e-mail: arias-bern@bluewin.ch)

M. A. Coplan, A. B. Galvin, G. Gloeckler, and F. M. Ipavich, Department of Physics and Astronimy, University of Maryland, College Park, MD 20742.
(e-mail: ipavich@umtof.umd.edu)

J. Geiss and R. Kallenbach, Internatinal Space Science Institute, CH-3012 Bern, Switzerland. (e-mail: reinald.kallenbach@soho.unibe.ch)

F. Gliem and K.-U. Reiche, Institut für Datenverarbeitung, Technische Universität Braunschweig, D-38023 Braunschweig, Germany. (e-mail: gliem@ida.ing.tu-bs.de)

K. C. Hsieh, Department of Physics, University of Arizona, Tuscon, AZ 85721. (e-mail: hsieh@soliton.physics.arizona.edu)

D. J. Judge and H. S. Ogawa, Space Science Center, University of Southern California, Los Angeles, CA 90089.
(e-mail: djudge@lism.usc.edu)

D. Hovestadt, B. Klecker, H. Kucharek, and M. Scholer, Max-Planck-Institut für extraterrestrische Physik, D-85740 Garching, Germany. (e-mail: hak@mpe-garching.mpg.de)

M. A. Lee and E. Möbius, Institute for the Study of Earth, Ocean and Space, University of New Hampshire, Durham, NH 03824. (e-mail: moebius@rotor.sr.unh.edu)

G. G. Managadze and M. I. Verigin, Institute for Space Physics, Moscow, Russia. (e-mail: gmanagad@esoc.bitnet)

M. Neugebauer, Jet Propulsion Laboratory, Pasadena, CA 91103. (e-mail: mneugebauer@jplsp.jpl.nasa.gov)

(Received March 2, 1998; revised July 7, 1998;
accepted July 23, 1998.)